Lab on a Chip

Cite this: *Lab Chip*, 2012, **12**, 309

www.rsc.org/loc

PAPER

A robust diffusion-based gradient generator for dynamic cell assays†

Javier Atencia,* Gregory A. Cooksey and Laurie E. Locascio

Received 31st August 2011, Accepted 31st October 2011
DOI: 10.1039/c1lc20829b

This manuscript describes a new method to generate purely diffusive chemical gradients that can be modified in time. The device is simple in its design and easy to use, which makes it amenable to study biological processes that involve static or dynamic chemical gradients such as chemotaxis. We describe the theory underlying the convection-free gradient generator, illustrate the design to implement the theory, and present a protocol to align multiple layers of double sided tape and laminates to fabricate the device. Using this device, a population of mammalian cells was exposed to different concentrations of a toxin within a concentration gradient in a 48 h experiment. Cells were probed dynamically by cycling the gradient on and off, and cell response was monitored using time-lapse fluorescence microscopy. The experiment and results illustrate the type of applications involving dynamic cell behavior that can be targeted with this type of gradient generator.

Introduction

Cells *in vivo* are exposed to an external microenvironment that they both sense and modify, with dynamic interactions that are impossible to elucidate from static *in vitro* experiments.[1] In order to understand the different temporal processes that regulate cell response to a dynamic environment, it is important to develop new assays to monitor and probe cells in the presence of time-evolving environmental perturbations, which are often chemical cues. Conventional *in vitro* cell toxicity and drug discovery assays are, in contrast, static: cells are exposed to a constant drug concentration, and the results are evaluated as a single measurement at the end of the experiment. We are interested in developing tools to probe cells with dynamic diffusive chemical cues. This approach could improve cell assays and mathematical predictions with better quantitative information about cell function in time.

There are two main microfluidic approaches to generate soluble chemical cues with spatio-temporal control:[2–5] convection-based and diffusion-based gradient generators. In convection-based gradient generation,[6,7] a chemical gradient is formed upstream by splitting and recombining reagents and buffers. Laminar flow at high Peclet number (convection dominates over diffusion) ensures that the chemical gradient is preserved downstream so that the chemical distribution is predictable and the assay is reproducible. However, fluid flow introduces shear on the cell environment, and removes soluble factors important in cell-cell communication and in cell autoregulation.[2]

Diffusion-based gradient generators rely on sources and sinks of diffusible signals to create chemical gradients in the absence of convection. These gradients preserve cell-cell communication and are shear free. Several approaches have been proposed to generate diffusion-based chemical gradients, among which using membranes or balancing pressure among sources and sinks are the most common. Membranes and hydrogels[8,9] can be used to block convection in microfluidic chambers while allowing free diffusion through them. However, membranes have lower diffusion constants than water, and inclusion of hydrogels usually requires greater distance between source and sink. As a result, in both cases the time required to establish a gradient increases, which directly affects how fast a dynamic soluble signal can be generated or modified.[10,11] The other main approach to creating a convection-free diffusion gradient in a microfluidic system is accomplished by ensuring that all inlets and outlets in the system experience exactly the same pressure. Membrane-less pressure balance is difficult to achieve practically, and current approaches compromise the robustness of the gradient or utilize devices with complex geometries that may be difficult to operate.[12–15]

Here we introduce a new microfluidic chip capable of generating diffusive chemical gradients, where the key is its simplicity. The unique design of the chip leverages the inherent pressure balance at the cross section of a microchannel under laminar flow to produce controlled diffusive chemical gradients without membranes. The main features of this design include the following: (*i*) it allows for dynamic control over the gradient; (*ii*) it renders the chemical gradient inherently robust to pressure fluctuations; (*iii*) it does not disrupt cell-cell communication *via* soluble signals; and (*iv*) it is simple to operate making it useful for

Biochemical Science Division, NIST, Gaithersburg, USA. E-mail: jatencia@nist.gov; Tel: (+301) 975-3589

† Electronic supplementary information (ESI) available: Video S1, Evolution of a chemical gradient; Video S2 Evolution of GFP intensity per region inside a buried channel; Video S3 Cell migration; and Fig. S1 Exploded view of the microfluidic chip. See DOI: 10.1039/c1lc20829b

mammalian cells assays. In addition, the gradient generator can be fabricated using low cost materials, *e.g.* plastic films, double sided tape, and rapid prototyping with a desktop razor cutter.

To illustrate the application of the device to a real-time cell-based assay, we used the gradient generator in combination with time-lapse fluorescent microscopy to monitor green fluorescent protein (GFP) expression by cells exposed to an intermittent chemical gradient of cycloheximide (CHX), an inhibitor of protein synthesis.[16]

Theory

Consider a microchannel of constant cross section filled with an incompressible liquid, where the flow is laminar and fully developed. In this case the velocity will be purely axial (x direction, see Fig. 1A) and the momentum equation[17] reduces to:

$$0 = -\frac{\partial \hat{p}}{\partial x} + \mu\left(\frac{\partial^2 u}{\partial y^2} + \frac{\partial^2 u}{\partial z^2}\right) \quad (1)$$

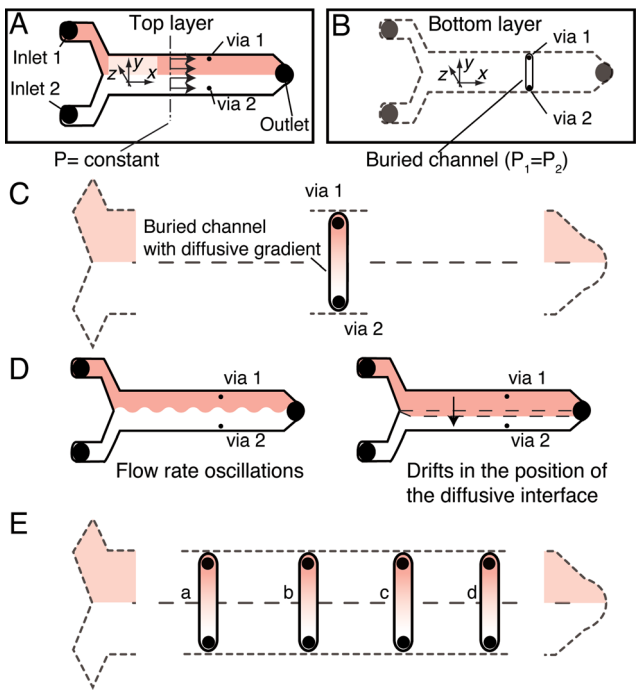

Fig. 1 In fully developed laminar flow in a straight channel, the pressure is constant at each cross section, eqn (2)–(3). (A) Vias located at the same cross section in the main channel (top layer) connect the channel to a buried channel in the bottom layer (B). The position of the vias ensures identical pressure in both, and purely diffusive mass transport in the buried channel. (C) When two miscible liquids flow side by side in the upper layer, the vias sample full concentration of the co-flowing streams, resulting in a diffusive chemical gradient inside the buried channel. (D) Since the vias are located away from the diffusive interface between co-flowing streams, the gradient is robust to oscillations in the flow rate or drifts in the position of the interface. (E) If several independent buried channels (a, b, c, d) are displayed subsequently along the length of the main channel, each buried channel will sample the same full chemical concentrations, and identical linear gradients should form enabling multiple experimental replicates to be performed within the same device.

$$0 = -\frac{\partial \hat{p}}{\partial y} \quad (2)$$

$$0 = -\frac{\partial \hat{p}}{\partial z} \quad (3)$$

where $\hat{p}$ is the total hydrostatic pressure, μ is the dynamic viscosity, u the velocity in the '*x*' direction, See Fig. 1A. These equations indicate that the pressure only varies along the x coordinate, and therefore, the pressure value at any point within a given cross section is identical and independent of the velocity profile.

Fig. 1A and B show a schematic layout of the conceptual design. In the top layer, two fluids of different solute concentration flow through a microchannel with a 'T' configuration (Fig. 1A). Vias (through-holes) located at the same 'x' and different 'y' positions, connect the microchannel in the top layer with a buried channel in the bottom layer (Fig. 1B). Since the vias are located at the same cross section, their pressure is inherently balanced and mass transport between them through the buried channel is purely diffusive (Fig. 1C). Additionally, the vias are located away from the diffusive interface, which makes the chemical gradient robust to drifts or oscillations in the position of the interface, (Fig. 1D). Fig. 1E shows a conceptual design where four independent buried channels are displayed along the main channel. Because each buried channel samples the same full chemical concentrations, identical linear gradients are formed, enabling multiple experimental replicates to be performed within the same device.

The main challenge of using this multilayer design for cell assays is practical, *i.e.* priming the microfluidic device and seeding cells in the buried channels. We overcome this challenge by introducing a new fabrication and cell loading protocol, which is described in the material and methods section.

Material and methods‡

Device fabrication

The fabrication protocol is based on techniques that were introduced by Bartholomeusz *et al.*[18] and adapted by Yuen *et al.*[19] to generate microfluidic devices using adhesive and plastic laminates cut with a razor cutter. Here, we adapt these protocols for the rapid fabrication and alignment of multilayer devices using 'alignment tabs'.

The devices used in the experiments were composed of 7 cut-out laminates assembled in 2 sections: the first section forms the bottom layer with buried channels and the second section forms the top layer with the main channel.

The bottom section of the device was fabricated by stacking cut-out layers of double-sided tape, polystyrene and double-sided tape onto a glass slide. The first adhesive layer was cut to have four 600 μm wide and 3 mm long channels to form the buried channels. The layer was adhered to a glass slide and its

‡ Certain commercial equipment, instruments or materials are identified in this report to specify adequately the experimental procedure. Such identification does not imply recommendation or endorsement by the National Institute of Standards and Technology, nor does it imply that the materials or equipment identified are necessarily the best available for the purpose.

upper protective liner was partially removed from the adhesive (Fig. 2A). The polystyrene layer was cut to have 750 μm diameter holes to form the vias (which effectively creates a 1.5 mm long buried channel), and was also perforated to create a foldable 'alignment tab'. The underside of this polystyrene layer (the ceiling of the buried channel) was sputtered with a 100 nm gold layer to block autofluorescence of the plastic from contributing to the background of the cell assay within the buried channel. The vias in the polystyrene layer were aligned over the buried channels, and the tab was pressed back to adhere to the exposed adhesive on the lower layer, see Fig. 2B. Subsequently the remainder of the protective liner was removed from the tape and the polystyrene layer was folded back down and stuck to the adhesive. (see Fig. 2C–E). The same procedure using an alignment tab was used to adhere a layer of double-sided tape cut out to define the main channel (Fig. 2F). Inclusion of this layer on the bottom section of the chip improves adhesion with the top section following cell loading.

The top section of the device, comprising the upper half of the main channel, was fabricated similarly using tabs to stack alternating double-sided tape and mylar film. The main channel was 320 μm tall × 1.5 mm wide with two 1 mm diameter inlets and one outlet. The top section (a layer of double-sided tape, mylar, double-sided tape, and the mylar lid) was stuck in place on the tabbed area of the bottom layer but was not closed until after cell loading and attachment, Fig. 3A (see an exploded view of the whole device in ESI, Fig. S1†).

The concept of alignment tabs was used to keep the top section and bottom section of the chip open so that cells could be loaded in the buried channels prior to use (Fig. 3). Before use, the device was placed inside a sealed glass Petri dish and exposed to UV light overnight with an Omnicure Series 2000 (Exfo) for sterilization.

All of the layers of the chip were pattern-cut with a plotter razor cutter (FC800, Graphtech). Double-sided tapes (40 μm thick, ARcare® 8890, Adhesives Research) were used as adhesive layers. Polystyrene films 100 μm thick were purchased from Griff Paper&Film and mylar films 200 μm thick were purchased from CAD/Art Services, Inc.

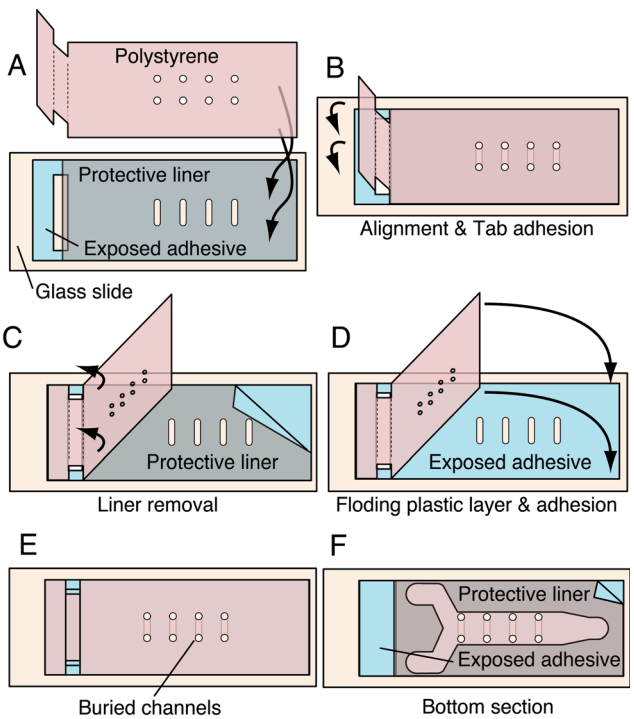

Fig. 2 Protocol for assembling a multilayer chip using 'alignment tabs'. (A) Assembly of the bottom section of the device starts by adhering one side of the double-sided tape layer containing the cut-out buried channels to a glass slide. The protective liner on the top of the alignment tab portion of the tape is removed to expose the adhesive. (B) A plastic layer with corresponding alignment tab and containing the vias is placed over the buried channels. (C) Once aligned, the tab is folded down and adhered to the exposed adhesive. (D) The remaining liner covering the buried channels is removed, and the plastic layer is folded down to register the vias with the buried channels. (E) The buried channels are complete. (F) A new layer of double sided tape containing the main channel is registered and adhered to the plastic with the same protocol using alignment tabs. At this point the bottom section of the chip is complete and ready to be adhered to the top section (see ESI, Fig. S1†).

Cell loading

Prior to cell seeding, a solution of 100 μg ml^{-1} fibronectin (F1141; Sigma-Aldrich) in phosphate buffered saline (PBS; Invitrogen) was pipetted into in each buried channel, and incubated at room temperature for 30 min. The solution was subsequently rinsed with culture media using passive pumping.[20,21] The culture media consisted of CO_2-independent media (RR060041; Invitrogen) supplemented with 10% fetal bovine serum (FBS; Invitrogen), 2% bovine serum albumin (BSA; Sigma-Aldrich), and 1% penicillin-streptomycin and Fungizone®, (PSF; Invitrogen). A suspension of 3.5 × 10^6 cells ml^{-1} of Vero cells (ATCC #CCL-81; transfected with dsEGFP; see.[22]) in culture media was introduced into the buried channels using a pipettor and passive pumping. The chip was then placed in an incubator at 37 °C and 90% relative humidity for 30 min to promote cell adhesion. Subsequently, the upper and lower surfaces of the main channel were wetted with culture media to prevent air bubbles during filling of the device. Excess fluid was removed, the liners were taken off, and the two layers of the chip were sealed together.

Magnetic connectors[23] and 0.5 mm ID TFE Teflon tubing (inlet) (Supelco) or 0.254 mm ID Tygon® tubing (outlet) (Cole-Parmer, IL, USA) were used to interface the device with pressurized containers.[24] The driving pressure was controlled using Matlab (The Mathworks, Inc.) and a digital pressure driver (Alicat Scientific, AZ, USA). The total flow rate was monitored by weighing the waste reservoir positioned on a microbalance (AP1105; Ohaus Corp, NJ, USA). The microbalance was placed about 1 m higher than the reservoirs to provide backpressure and to prevent bubble formation within the device.

To perform the dynamic cell assays, cycloheximide (Sigma-Aldrich) was diluted to 1.0 μg mL^{-1} (3.6 μmole/L) in culture medium from 100 mg mL^{-1} stock solution in dimethyl sulfoxide (Sigma-Aldrich).

Microscopy and image analysis

Time-lapse fluorescence microscopy was performed using an inverted microscope (Axio Observer Z1; Carl Zeiss

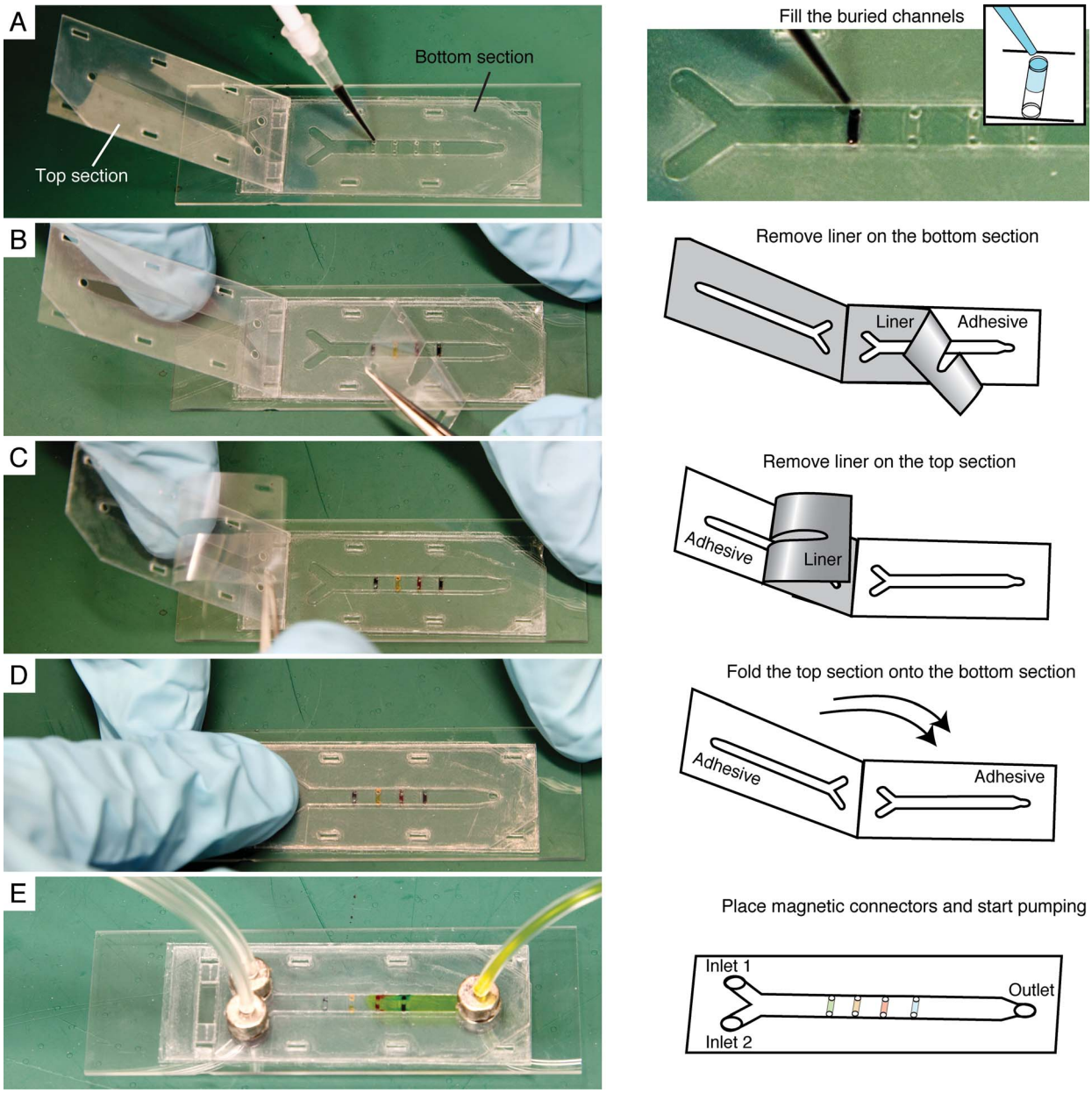

Fig. 3 Device loading. The top section of the chip is initially open to facilitate loading of the buried channels with cells. (A) Solutions can be introduced in the buried channels by direct pipetting, using capillary forces, or by passive pumping. (B) After the buried channels are filled, the liner from the bottom section of the chip is removed leaving the adhesive face exposed; (C) likewise the protective liner covering the adhesive in top section of the chip is removed, (D) and the lid is folded down against the bottom section of the chip. The alignment tab works as a hinge and ensures that both sides of the chips are aligned. (E) Finally, magnetic connectors are placed on the outlet and inlets,[23] and liquid is pumped in the chip, initially through the outlet first to facilitate controlled priming, and subsequently through the inlets.

MicroImaging, Inc.) with an automated mechanical stage, enclosed in a heated chamber (37 °C). Grayscale images were acquired with a 20x objective in the case of cell assays and a 5x objective for the gradient characterization. Images were analyzed using Matlab.

For gradient characterization the intensity values were normalized as[25]

$$\vec{I}_{norm}(t) = 100 \cdot (\vec{I}(t) - \vec{I}_0)/(\vec{I}_f - \vec{I}_0) \quad (4)$$

where $\vec{I}(t)$ is a vector containing the pixel intensity along the line at each time lapse, $\vec{I}_0$ is the vector of intensity along the line with no fluorescein, and $\vec{I}_f$ is the vector of the pixel intensity along the line when the whole channel is filled with fluorescein solution.

For the dynamic cell assays, the average intensity in each region was calculated as

$$I(t) = \frac{I_{av}(t) - I_{\min}(t)}{I_{av}(t_0) + I_{\min}(t_0)} * I_{corr}(t) \quad (5)$$

where $I(t)$ is the normalized average intensity, $I_{av}(t)$ is the average intensity value in the region, $I_{\min}(t)$ the minimum intensity value in the region which accounts for background, t_0 is the time that is

used as reference for normalization, and $I_{corr}(t)$ is a vector that accounts for the drift in the intensity of the illumination lamp over time. Its value was calculated as

$$I_{corr}(t) = \frac{I_{background}(t_0) - I_{DarkCounts}}{I_{background}(t) - I_{DarkCounts}} \quad (6)$$

Results & discussion

The design utilized in these experiments had four buried channels along the length of the main channel. Each buried channel was perpendicular to the direction of the flow in the main channel (see Fig. 1E). First we validated the formation of a linear gradient and then we performed a dynamic cell assay exposing a population of Vero cells to an intermittent chemical gradient of cycloheximide (CHX).

Gradient generation

The generation of a linear diffusive chemical gradient inside the buried channels was validated experimentally. Fluorescein solution and water were introduced into the main channel of the chip through the inlets at 15 μl min^{-1} each, resulting in an average velocity in the main channel of 0.34 mm s^{-1} and Reynolds number Re = 0.25. A diffusive interface formed between streams along the middle of the main channel, and away (≈0.75 mm) from the side walls; ensuring the vias on one side of the interface were exposed only to fluorescein, and the vias on the other side were exposed only to water.

We monitored the evolution of fluorescence intensity inside the buried channels using time-lapse fluorescence microscopy (see ESI, video S1†). Pixel intensity along a 10-pixel wide line connecting the two vias in each image was evaluated every 5 min using Matlab. The intensity values were normalized between 0%, when no fluorescein was present in the channel, and 100% with the buried channel was filled with the maximum concentration of fluorescein (acquired at the end of the experiment after stopping the flow of water).[25] The gradient formed fully in ≈30 min, with a time constant of $\tau_{\text{gradient formation}} \approx 13$ min. Once developed, the gradient was linear and stable (Fig. 4). The linearity of the gradient is indicative of the absence of convection in the buried channels.[26] We also introduced 4 μm fluorescent beads that were used as flow path tracers using long time exposure acquisition. None of the beads entered the buried channels, which further confirms the absence of convection.

Dynamic cell assays

To demonstrate a dynamic cell assay, the microfluidic chip was used to deliver a gradient of CHX, a ribosomal inhibitor, across a population of ds-EGFP Vero cells. The cells were transfected with an enhanced GFP construct that includes a constitutively active promoter and a proteasome targeting sequence.[22] Thus, the cells exhibit a GFP intensity related to the balance between protein expression and degradation. If GFP production decreases or stops, the accumulated GFP degrades until a new equilibrium is met. Exposure of this cell line to CHX was previously demonstrated as a model system for toxicity assays.[22,27,28]

The CHX gradient was switched on and off three times in 43 h, and ribosomal activity was monitored over time as function of cellular GFP production and accumulation. During the recovery phase (no toxin), culture media was continuously perfused through both inlets to the main channel.

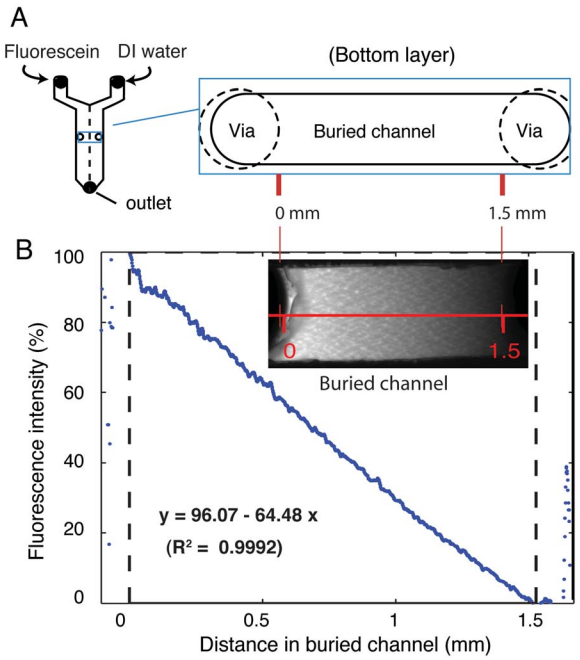

Fig. 4 Steady-state gradient across the buried channel. (A) Schematic showing the gradient characterization within the buried channel. Inlets were perfused with 1 mmol L^{-1} fluorescein solution and deionized water at the same flow rate. (B) The fluorescent intensity is shown as measured along a 1.5 mm line connecting both vias inside the buried channel (inset). The value of the light intensity reached 90% of the steady state value in ≈30 min, see ESI, video S1.†

Quantification of cellular dynamics. Fig. 5 shows fluorescence images from various time-points throughout the experiment corresponding to sequential non-lethal doses of CHX and washes. To quantify the cellular response to CHX, we divided the interior of the buried channels into 10 equally sized convection-free regions (regions 2–11) representing different samples of the CHX gradient when the gradient was switched on. Based upon the fluorescein measurements performed to validate the linearity of the gradient, we assume that CHX concentration varied linearly from 0.95 μg ml^{-1} ± 0.05 μg ml^{-1} (values are given as mean ± 1 standard deviation) in region 2 to 0.05 g ml^{-1} ±0.05 μg ml^{-1} in region 11. Qualitatively, decrease in cell fluorescence commenced quickly following the introduction of CHX in the left *via* (region 1). Fluorescence of cells on the left side of the buried channel was reduced most compared to cells on the right side of the buried channel and the CHX-free *via* (region 12). Cell recovery after washing away CHX on the left side of the main channel was demonstrated by increased brightness; see ESI, video S2.†

Cellular dynamics and GFP expression. In order to compare the dynamics of GFP intensity independently of cell density, we computed the average pixel intensity in each region throughout the experiment, and normalized to the value at the beginning of

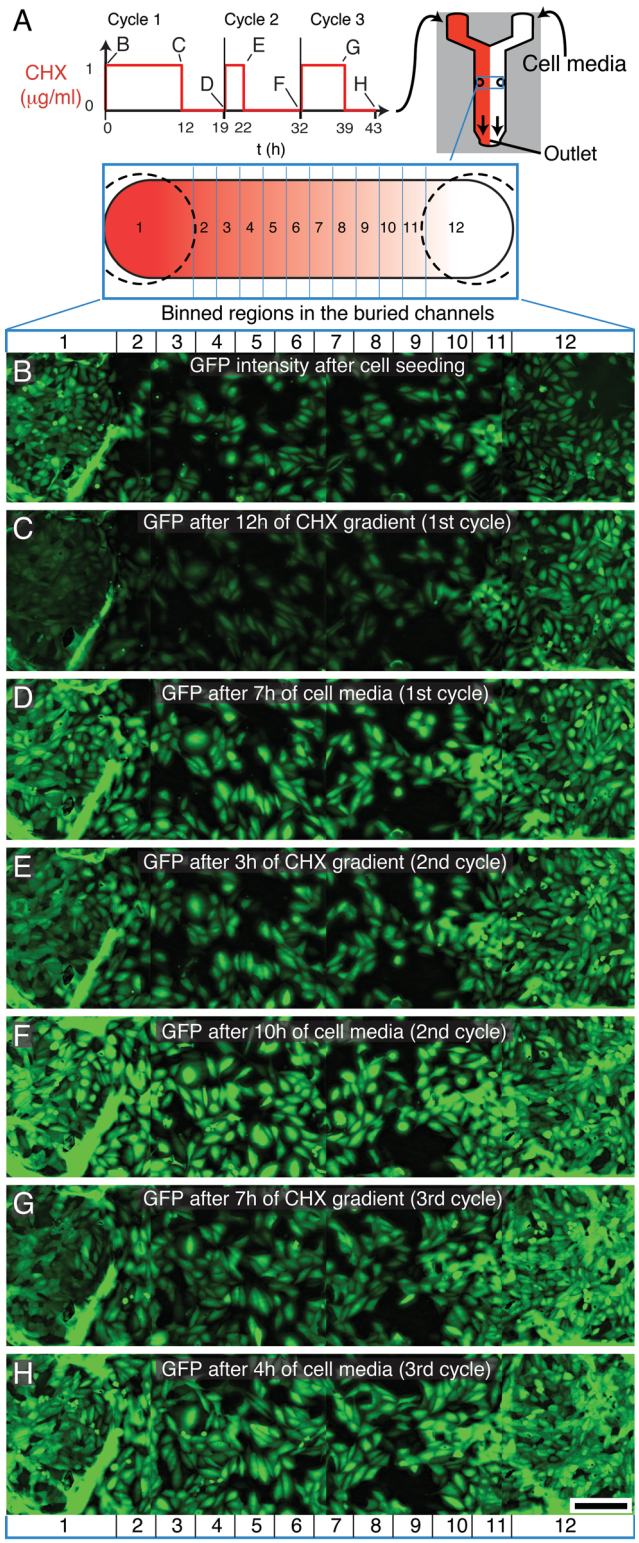

Fig. 5 (A) Timeline of the cell assay under dynamic chemical gradient. A population of Vero cells growing in the buried channels was exposed to three cycles of CHX. For analysis, the buried channel was divided into 10 regions within a linear distribution of CHX concentration ranges (B–H) Fluorescence micrographs of the evolution of GFP intensity inside the buried channel throughout the experiment. Each micrograph shows a snapshot of the GFP at given times, after exposure to the CHX gradient, or after a cell recovery period. Scale bar is 200 μm.

the experiment. Fig. 6A shows the fluorescence intensity in each region over time (see also ESI, video S2†).

The intensity in region 12, the via without toxin, increased linearly through the experiment, with a slope of $(4.38 \pm 0.04 \times 10^{-2})$ h^{-1} (± 95% confidence bounds), and a doubling time of 22.8 h. These findings indicate that GFP expression by cells in Region 12 was not perturbed by toxin. Regions 1–11 experienced intensity decay when the gradient was switched on, and a linear increase of intensity when the gradient was off. The rate of GFP degradation was found by fitting the fluorescence traces during CHX exposure to the following equation:[29]

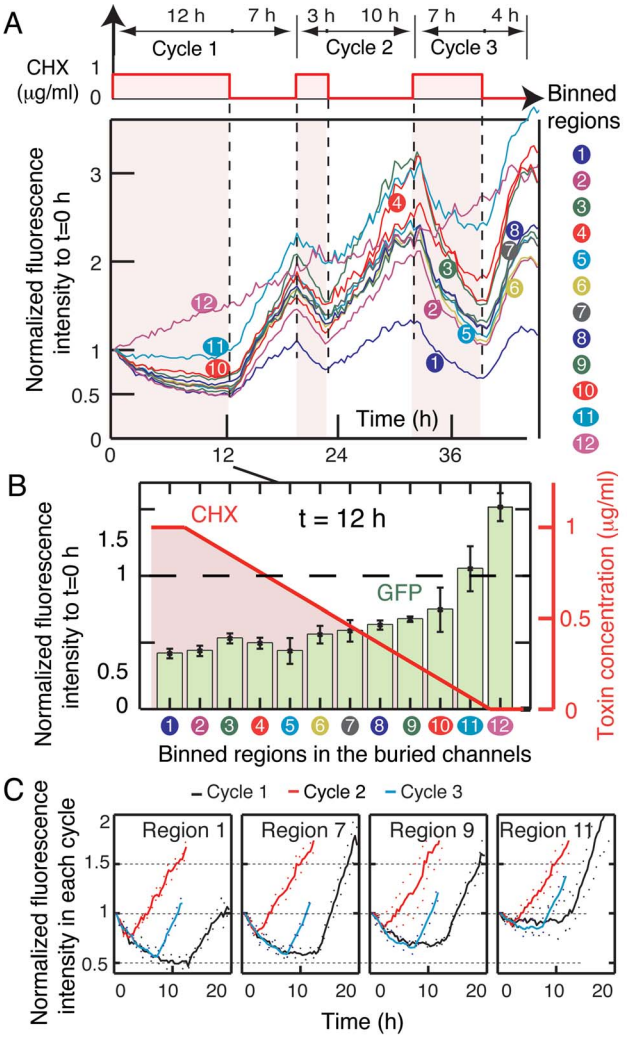

Fig. 6 (A) GFP accumulation in time for each binned- region (1 to 12) throughout three consecutive cycles of CHX exposure. Each colored curve indicates the normalized GFP intensity for a binned region averaged across three buried channels. Each curve was normalized to the beginning of the experiment. (B) GFP intensity in all regions after 12 h exposure to a linear CHX gradient in cycle 1. The CHX concentration within each region can be estimated along the red line using the right axis. (C) GFP intensity from each toxin cycle is overlaid from 4 different regions of the CHX concentration gradient. Black is cycle 1, red is cycle 2, and blue is cycle 3. Solid lines show the mean intensity from the three channels, and the dotted lines indicate the standard deviation.

$$I_{region}(t) = (1 - K)\cdot e^{-t/\tau_{GFPdelay}} + K \quad (7)$$

where $I_{region}(t)$ is the normalized average intensity in each region, $\tau_{GFP\ decay}$ is the time constant of the decay in intensity, and K is a constant indicative of GFP accumulation, and thus, the equilibrium between GFP production and degradation.

Regions 1–11 showed similar decay constants, $\tau_{GFP\ decay}$ = 3.69 h, ([3.18, 4.39] h; 95% confidence bounds), but reached a different steady state value of GFP intensity, K, according to their position within the CHX gradient (Fig. 6B). We assume that because the time constant of GFP decay was found to be an order of magnitude higher than the time constant of the gradient formation, both dynamics are decoupled and can be analyzed independently. These results suggest the production rate of GFP and ribosomal activity was affected by CHX concentration (constant term in fitted curves), but not protein degradation rate (exponential term in fitted curves) and, therefore, proteasome activity.

Cell migration and proliferation. We tracked the position of 220 cells inside one of the buried channels to account for cell migration between regions throughout the experiments (see ESI, video S3†). We did not observe directional migration as a consequence to toxin gradient (chemotaxis). We also monitored cell division to determine the potential impact of unbalanced proliferation or cell death in the results. We observed that while the distribution of doubling events in region 12 was independent of the cycles of toxin exposure, fewer cells appeared to divide during times of CHX exposure, but a connection to CHX concentration could not be established.

Cellular response to cyclic stimuli. To compare cell activity for each region in the different cycles, we normalized the GFP intensity within each region to the beginning of each toxin exposure. Fig. 6C shows traces from four regions in separate parts of the gradient, which correspond to the means of the three buried channels during each CHX exposure.

Interestingly, the results show similar trends in GFP decay during CHX exposure and GFP accumulation during cell recovery for the three cycles. As shown by the red curves in Fig. 6C, the trends in toxin response are similar despite different durations of toxin exposure and recovery. These results suggest that, if the degradation rate of GFP (exponential term in fitted curves) is independent of toxin concentration and is also known *a priori*, the dynamic cellular response to short cycles of toxin could be used to infer cell growth (protein production at equilibrium), and potentially cell fate in quicker toxicity assays (hours) than current conventional assays (days). Validation of this hypothesis would require further experiments with wider ranges of toxin concentrations.

Conclusions

We have introduced a simple microfluidic chip that can be used to generate diffusive cellular microenvironments with temporal control for dynamic cell assays. As illustration, the microfluidic chip was used to generate a linear dilution of a chemical across a population of cells. Although cells could have been tested in discrete vials using manual dilutions, the microfluidic chip provides temporal control over the gradient. Thus, by cycling the gradient on and off, cells exposed to different chemical concentrations were probed dynamically. The results from the dynamic toxicity experiments using Vero cells raise interesting biological questions such as the relationship between proteasome activity and protein accumulation, and potential linearity in cell responses that are beyond the scope of this manuscript.

There are some limitations of the new design that include the fact that it does not allow for multiple overlapping gradients[14]; and that gradient generation is slower than convection-based gradient generators. However, our design solves a critical challenge in the robustness and predictability of a diffusive gradient. Previous designs required exquisite symmetry in the fabricated designs while, in contrast, the approach introduced here is simple and easily reproduced.

In vitro assays involving cells exposed to diffusive temporal cues (chemical gradients with temporal control) could be used to model biological processes and gain insights that are difficult to infer with macroscale techniques. For example, it has been shown that diffusive chemical waves are utilized by human polymorphonuclear leukocytes,[30] *Dictyostelium discoidium*[31] and neutrophils[32] to enhance signals during coordinated migration towards a chemoattractant; the synchronization of cell-signal oscillations in *D. discoidium*[33] and yeast[34] have been shown to result in the emergence of group dynamics (*e.g.* dynamical quorum sensing[35,36]). Furthermore, temporal chemical cues are key elements in morphogenesis and organ growth.

We believe that the simplicity of the microfluidic chip and the robustness in the generation of dynamic chemical gradients will be useful to explore these and similar biological processes. Additionally, the ability to maintain chemical gradients for extended periods of time should be of interest to study cell migration for diagnostic applications related to the immune response and cancer metastasis.

Acknowledgements

We acknowledge John Elliott, Michael Halter, Anne Plant and Daniel Sisan for helpful discussions. We thank Connie Rogers-Newcome from Adhesive Research. Inc for providing double-sided tape samples. Part of this work was performed at the NIST Center for Nanoscale Science and Technology Nanofabrication facility that is partially sponsored by the NIST Office of Microelectronics Programs.

Notes and references

1 M. R. Bennett and J. Hasty, *Nat. Rev. Genet.*, 2009, **10**, 628–638.
2 T. M. Keenan and A. Folch, *Lab Chip*, 2008, **8**, 34–57.
3 J. Atencia and D. J. Beebe, *Nature*, 2005, **437**, 648–655.
4 T. Ahmed, T. S. Shimizu and R. Stocker, *Integr. Biol.*, 2010, **2**, 604–629.
5 S. Kim, H. J. Kim and N. L. Jeon, *Integr. Biol.*, 2010, **2**, 584–603.
6 S. K. W. Dertinger, D. T. Chiu, N. L. Jeon and G. M. Whitesides, *Anal. Chem.*, 2001, **73**, 1240–1246.
7 N. L. Jeon, H. Baskaran, S. K. W. Dertinger, G. M. Whitesides, L. Van de Water and M. Toner, *Nat Biotechnol*, 2002, **20**, 826–830.
8 S. Y. Cheng, S. Heilman, M. Wasserman, S. Archer, M. L. Shuler and M. M. Wu, *Lab Chip*, 2007, **7**, 763–769.
9 T. Ahmed, T. S. Shimizu and R. Stocker, *Nano Lett.*, 2010, **10**, 3379–3385.
10 V. V. Abhyankar, M. A. Lokuta, A. Huttenlocher and D. J. Beebe, *Lab Chip*, 2006, **6**, 389–393.

11 D. Kim, M. A. Lokuta, A. Huttenlocher and D. J. Beebe, *Lab Chip*, 2009, **9**, 1797–1800.
12 B. Mosadegh, C. Huang, J. W. Park, H. S. Shin, B. G. Chung, S. K. Hwang, K. H. Lee, H. J. Kim, J. Brody and N. L. Jeon, *Langmuir*, 2007, **23**, 10910–10912.
13 D. Irimia, G. Charras, N. Agrawal, T. Mitchison and M. Toner, *Lab Chip*, 2007, **7**, 1783–1790.
14 J. Atencia, J. Morrow and L. E. Locascio, *Lab Chip*, 2009, **9**, 2707–2714.
15 J. J. VanDersarl, A. M. Xu and N. A. Melosh, *Lab Chip*, 2011, **11**, 3057–3063.
16 H. L. Ennis and M. Lubin, *Science*, 1964, **146**, 1474.
17 F. M. White, *Viscous fluid flow*, McGraw-Hill Higher Education, New York, NY, 2006.
18 D. A. Bartholomeusz, R. W. Boutte and J. D. Andrade, *J. Microelectromech. Syst.*, 2005, **14**, 1364–1374.
19 P. K. Yuen and V. N. Goral, *Lab Chip*, 2010, **10**, 384–387.
20 G. M. Walker and D. J. Beebe, *Lab Chip*, 2002, **2**, 131–134.
21 J. Warrick, I. Meyvantsson, J. I. Ju and D. J. Beebe, *Lab Chip*, 2007, **7**, 316–321.
22 M. Halter, A. Tona, K. Bhadriraju, A. L. Plant and J. T. Elliott, *Cytometry, Part A*, 2007, **71A**, 827–834.
23 J. Atencia, G. A. Cooksey, A. Jahn, J. M. Zook, W. N. Vreeland and L. E. Locascio, *Lab Chip*, 2010, **10**, 246–249.
24 G. A. Cooksey, C. G. Sip and A. Folch, *Lab Chip*, 2009, **9**, 417–426.
25 S. G. Turney, S. M. Culican and J. W. Lichtman, *J. Neurosci. Methods*, 1996, **64**, 199–208.
26 H. C. Berg and L. Turner, *Biophys. J.*, 1990, **58**, 919–930.
27 M. Halter, J. L. Almeida, A. Tona, K. D. Cole, A. L. Plant and J. T. Elliott, *Assay Drug Dev Techn*, 2009, **7**, 9–10.
28 G. A. Cooksey, J. T. Elliott and A. L. Plant, *Anal. Chem.*, 2011, **83**, 3890–3896.
29 U. Alon, *An introduction to Systems Biology. Design Principles of Biological Cricuits*, Chapman & Hall/CRC, Boca Raton, 2007.
30 J. Geiger, D. Wessels and D. R. Soll, *Cell Motil. Cytoskeleton*, 2003, **56**, 27–44.
31 C. P. McCann, P. W. Kriebel, C. A. Parent and W. Losert, *J. Cell Sci.*, 2010, **123**, 1724–1731.
32 P. Alfonso and C. A. Parent, personal communication.
33 T. Gregor, K. Fujimoto, N. Masaki and S. Sawai, *Science*, 2010, **328**, 1021–1025.
34 S. De Monte, F. d'Ovidio, S. Dano and P. G. Sorensen, *Proc. Natl. Acad. Sci. U. S. A.*, 2007, **104**, 18377–18381.
35 A. F. Taylor, M. R. Tinsley, F. Wang, Z. Y. Huang and K. Showalter, *Science*, 2009, **323**, 614–617.
36 M. R. Tinsley, A. F. Taylor, Z. Huang, F. Wang and K. Showalter, *Phys. D*, 2010, **239**, 785–790.

